Asymmetries in the Earth's dayside magnetosheath: results from global hybrid-Vlasov simulations

Lucile Turc[1], Vertti Tarvus[1], Andrew Dimmock[2], Markus Battarbee[1], Urs Ganse[1], Andreas Johlander[1], Maxime Grandin[1], Yann Pfau-Kempf[1], Maxime Dubart[1], and Minna Palmroth[1,3]

[1]Department of Physics, University of Helsinki, Helsinki, Finland
[2]IRF-U, Uppsala, Sweden
[3]Finnish Meteorological Institute, Helsinki, Finland

Correspondence: Lucile Turc (lucile.turc@helsinki.fi)

Abstract. Bounded by the bow shock and the magnetopause, the magnetosheath forms the interface between solar wind and magnetospheric plasmas and regulates solar wind-magnetosphere coupling. Previous works have revealed pronounced dawn-dusk asymmetries in the magnetosheath properties. The dependence of these asymmetries on the upstream parameters remains however largely unknown. One of the main sources of these asymmetries is the bow shock configuration, which is typically

5 quasi-parallel on the dawn side and quasi-perpendicular on the dusk side of the terrestrial magnetosheath because of the Parker spiral orientation of the interplanetary magnetic field (IMF) at Earth. Most of these previous studies rely on collections of spacecraft measurements associated with a wide range of upstream conditions which are processed in order to obtain average values of the magnetosheath parameters. In this work, we use a different approach and quantify the magnetosheath asymmetries in global hybrid-Vlasov simulations performed with the Vlasiator model. We concentrate on three parameters: the magnetic

10 field strength, the plasma density and the flow velocity. We find that the Vlasiator model reproduces accurately the polarity of the asymmetries, but that their level tends to be higher than in spacecraft measurements, probably because the magnetosheath parameters are obtained from a single set of upstream conditions in the simulation, making the asymmetries more prominent. We investigate how the asymmetries change when the angle between the IMF and the Sun-Earth line is reduced and when the Alfvén Mach number decreases. We find that a more radial IMF results in a stronger magnetic field asymmetry and a larger

15 variability of the magnetosheath density. In contrast, a lower Alfvén Mach number leads to a reduced magnetic field asymmetry and a decrease in the variability of the magnetosheath density and velocity, the latter likely due to weaker foreshock processes. Our results highlight the strong impact of the foreshock on global magnetosheath properties, in particular on the magnetosheath density, which is extremely sensitive to transient foreshock processes.

1 Introduction

The interaction of the supermagnetosonic solar wind with the Earth's magnetosphere forms a standing bow shock which decelerates the incoming flow to submagnetosonic speeds in front of the obstacle. Extending between the bow shock and the magnetopause, the magnetosheath houses shocked solar wind plasma, which has been compressed and heated at the shock crossing. At the interface between the solar wind and the magnetosphere, the magnetosheath regulates the processes which transfer momentum and energy from the former to the latter and thus plays a key role in solar wind-magnetosphere coupling (Pulkkinen et al., 2016; Eastwood et al., 2017). Understanding and accurate modelling of this coupling therefore call for an in-depth knowledge of magnetosheath properties and their dependence on upstream solar wind parameters.

Since the early gasdynamic model of Spreiter et al. (1966), the magnetosheath has been subject to intensive scrutiny (e.g. Petrinec et al., 1997; Paularena et al., 2001; Longmore et al., 2005; Lucek et al., 2005; Dimmock and Nykyri, 2013; Lavraud et al., 2013; Dimmock et al., 2017). These studies revealed that the magnetosheath properties display significant spatial variations, as a function of the distance from the boundaries, with for example the formation of the plasma depletion layer near the magnetopause during northward interplanetary magnetic field (IMF) conditions (e.g. Wang et al., 2004), and as a function of the distance from the Sun-Earth line, with pronounced dawn-dusk asymmetries (see the reviews by Walsh et al., 2014; Dimmock et al., 2017, and references therein). One of the main sources of these dawn-dusk asymmetries is the bow shock. The shock properties depend strongly on the angle θ_{Bn} between the IMF and the local normal to the shock's surface. Because of the Parker-spiral orientation of the IMF at Earth, which makes a $45°$ angle with the Sun-Earth line, the dusk side of the magnetosheath generally lies downstream of a quasi-perpendicular ($Q_\perp$) shock ($\theta_{\mathrm{Bn}} > 45°$), while the dawn side is associated with a quasi-parallel ($Q_\parallel$) shock ($\theta_{\mathrm{Bn}} < 45°$). Even in the fluid approximation, these contrasted shock regimes result in different plasma properties in the downstream region. Using the Rankine-Hugoniot jump conditions, Walters (1964) found larger plasma densities and temperatures downstream of the quasi-parallel shock than downstream of the quasi-perpendicular shock. Global magnetohydrodynamic (MHD) simulations have brought additional support to the dawn magnetosheath being home to a hotter and denser plasma, while the magnetic field strength and flow velocity are larger on the dusk flank (Walsh et al., 2012).

Investigating magnetosheath asymmetries using spacecraft measurements is a challenging task because it requires an extensive spatial coverage of this region. Since simultaneous measurements in different parts of the magnetosheath are scarce, most observational studies rely on compilations of spacecraft observations from different passes through this region to build statistical maps of the magnetosheath properties (Paularena et al., 2001; Němeček et al., 2002; Longmore et al., 2005; Walsh et al., 2012; Dimmock and Nykyri, 2013). The main drawbacks of this approach are that these data are collected during vastly different upstream conditions and that the position of the spacecraft relative to the magnetosheath boundaries is essentially unknown. The former issue is generally addressed by normalising the magnetosheath parameters with their solar wind counterparts, while empirical models of the magnetosheath boundaries provide an estimate of the relative position of the spacecraft inside the magnetosheath.

Consistent with the aforementioned theoretical and numerical works, observational studies have reported a dusk-favoured asymmetry of the magnetic field strength and of the plasma velocity (Longmore et al., 2005; Walsh et al., 2012; Dimmock

and Nykyri, 2013; Dimmock et al., 2017). The ion temperature, on the other hand, showcases a dawn-favoured asymmetry,
55   probably due to enhanced heating at the more turbulent quasi-parallel shock (Walsh et al., 2012; Dimmock et al., 2015a).
Furthermore, magnetic field and velocity fluctuations are stronger in the dawn magnetosheath (Dimmock et al., 2014, 2016a),
while temperature anisotropy and mirror mode wave activity are more prominent in the dusk sector (Dimmock et al., 2015b;
Soucek et al., 2015).

The density asymmetry turned out to be more elusive in spacecraft measurements. Though a clear dawn-favoured asymmetry
60   was found in several data sets (Paularena et al. (2001) for solar maximum; Němeček et al. (2002); Walsh et al. (2012); Dimmock
et al. (2016b)), others did not display any significant asymmetry levels (Dimmock and Nykyri, 2013; Paularena et al., 2001,
for solar minimum), or even an asymmetry with a changing polarity depending on the location inside the magnetosheath
(Němeček et al., 2003; Longmore et al., 2005). We note that because they originate from different spacecraft missions, the data
sets used in these studies cover various parts of the magnetosheath: nightside (Paularena et al., 2001), close to the terminator
65   (Němeček et al., 2002, 2003), dayside at high latitudes (Longmore et al., 2005), and dayside near the equatorial plane, either
near the magnetopause (Walsh et al., 2012; Dimmock et al., 2016b) or across the whole magnetosheath thickness (Dimmock
and Nykyri, 2013). They also correspond to various parts of the solar cycle, which may affect the level of the density asymmetry
because the average solar wind parameters depend on solar activity. However, opposite behaviours were reported by Paularena
et al. (2001) and Dimmock et al. (2016b).

70   The dependence of magnetosheath asymmetries on upstream parameters can bring insight into the processes that create them.
Longmore et al. (2005) and Dimmock et al. (2017) found no clear dependence of the density and velocity asymmetries on the
IMF direction, suggesting that they may not be driven by the bow shock. On the other hand, the level of these asymmetries
increases with the Alfvén Mach number (M_A), as does the temperature asymmetry, according to the numerical simulations
performed by Walsh et al. (2012). They also show that an increasing M_A would also tend to increase the magnetic field
75   strength asymmetry. Walsh et al. (2012) ascribe the observed density asymmetry to the asymmetric bow shock shape, as its
quasi-parallel sector lies closer to the magnetopause than its quasi-perpendicular sector. They argue that the apparent lack of
dependence of the density asymmetry on the IMF direction in statistical studies is likely due to the limited number of data
points associated with non-Parker-spiral IMF orientations. As evidenced by these contradicting claims, many open questions
remain regarding the precise sources of the observed magnetosheath asymmetries and their dependence on upstream solar wind
80   conditions.

Asymmetries in the magnetosheath parameters result in turn in an asymmetric magnetospheric driving. Large amplitude
velocity fluctuations in the magnetosheath are conducive to a faster growth of the Kelvin-Helmholtz instability at the Earth's
magnetopause and larger plasma transport through the boundary (Nykyri et al., 2017). These processes would thus favour
the quasi-parallel flank. Also, ions of magnetosheath origin in the plasma sheet present a dawn-favoured asymmetry of about
85    $30-40\%$ (Wing et al., 2005). This asymmetry could partially be explained by the temperature asymmetry in the magnetosheath,
while additional heating processes may be regulated by the asymmetric distribution of other magnetosheath parameters (Dim-
mock et al., 2015a; Dimmock et al., 2017).

Numerical simulations can help shed new light onto magnetosheath asymmetries, as they provide a global view of the magnetosheath for a given set of solar wind conditions, instead of relying on statistical maps constructed from measurements associated with a variety of upstream parameters. This also removes possible errors when determining the context of magnetosheath measurements, which must be combined with time-lagged data from an upstream monitor in observational studies. To date, most numerical studies of magnetosheath asymmetries have used MHD models (Walsh et al., 2012; Dimmock and Nykyri, 2013), though the temperature asymmetry was qualitatively compared with the outputs from a hybrid-Particle-in-Cell simulation by Dimmock et al. (2015a). The physics of the quasi-parallel bow shock and its associated foreshock are however inherently kinetic in nature, and thus a kinetic approach is warranted to study magnetosheath parameters downstream of the quasi-parallel shock.

In this paper, we present the first analysis of magnetosheath asymmetries as obtained from global ion kinetic simulations performed with the hybrid-Vlasov model Vlasiator (von Alfthan et al., 2014; Palmroth et al., 2018). We use a set of three different runs to investigate the effects of the IMF cone angle θ_{Bx} (measured between the IMF vector and the Sun-Earth line) and the solar wind Alfvén Mach number, which are key parameters controlling the shock properties. In this first study based on hybrid-Vlasov simulations, we choose to focus on three primary magnetosheath parameters: the magnetic field strength B, the plasma velocity V and the ion density n_{p}. For the latter, we will attempt to identify possible reasons for its large variability in observational studies.

2 Methodology

2.1 The Vlasiator simulation

Vlasiator is a hybrid-Vlasov model designed to perform global simulations of the Earth's plasma environment while retaining ion kinetic physics (von Alfthan et al., 2014; Palmroth et al., 2018). In the hybrid-Vlasov formalism, ions are treated as velocity distribution functions evolving in phase space whereas electrons are modelled as a cold massless charge-neutralising fluid. The temporal evolution of the system is obtained by solving Vlasov's equation, coupled with Maxwell's equations. Ohm's law, including the Hall term, provides closure to the system. In Vlasiator, the use of realistic proton mass and charge, together with the full strength of the Earth's dipole field, results in processes being simulated at their actual physical scales, as encountered in near-Earth space. This makes the comparison with spacecraft measurements straightforward.

The runs presented in this paper are two-dimensional (2D) in ordinary space. Each grid cell in ordinary space is self-consistently coupled with a 3D velocity space in which the ion distribution functions evolve. The coordinate system used in the simulation is equivalent to the Geocentric Solar Ecliptic (GSE) reference frame. In this Earth-centred frame, the x-axis points towards the Sun, z is perpendicular to the Earth's orbital plane and points northward, and y completes the right-handed triplet. Depending on the runs, the simulation domain covers either the equatorial $(x-y)$ or the noon-midnight meridional $(x-z)$ plane (see Table 1 for a summary of the run parameters). In equatorial runs, we use the Earth's magnetic dipole with its actual value of $8.0 \times 10^{22} \mathrm{A\,m^2}$, while for runs in the noon-midnight meridional plane, a 2D line dipole is used (Daldorff et al., 2014). In all runs, the solar wind flows into the simulation domain from the $+x$ edge. Copy conditions are applied at the other walls

Table 1. Summary of the run parameters

Run name	Simulation plane	IMF cone angle $\theta_{\mathrm{B}x}$	IMF strength	$\mathrm{M_A}$	$n_{\mathrm{SW}}\,[\mathrm{cm}^{-3}]$	$\mathbf{V}_{\mathrm{SW}}\,[\mathrm{km\,s^{-1}}]$
Run 1	$x-z$ plane	$45°$	5 nT	6.9	1	$(-750,0,0)$
Run 2A	$x-y$ plane	$30°$	5 nT	6.9	1	$(-750,0,0)$
Run 2B	$x-y$ plane	$30°$	10 nT	3.5	1	$(-750,0,0)$

of the simulation domain, while periodic conditions are employed for the out-of-plane cell boundaries (i.e., in the z direction for a run in the $x-y$ plane). The inner boundary of the simulation domain is a circle at about $4.7\,\mathrm{R_E}$ from the Earth's centre, considered a perfect conductor.

2.2 Runs used and analysis method

125 In this study, we analyse three Vlasiator runs, each corresponding to different IMF conditions (see Table 1). This allows us to investigate the influence of the IMF orientation and strength (and by extension the Alfvén Mach number) on magnetosheath asymmetries. In all three runs, the solar wind ions are injected at the inflow boundary as a Maxwellian population with a density $n_{\mathrm{SW}} = 1\,\mathrm{cm}^{-3}$ and a temperature $T_{\mathrm{SW}} = 0.5\mathrm{MK}$, flowing at a velocity $\mathbf{V}_{\mathrm{SW}} = (-750,0,0)\,\mathrm{km\,s^{-1}}$, thus corresponding to fast solar wind conditions.

130 In the reference run, hereafter Run 1, the IMF vector makes a $45°$ cone angle with the Sun-Earth line and lies in the $x-z$ plane, with $\mathbf{B} = (3.54, 0., -3.54)\,\mathrm{nT}$. This run simulates the noon-midnight meridional plane of near-Earth space, as it was initially designed to study e.g. dayside and nightside reconnection in the presence of the foreshock (Hoilijoki et al., 2019). For an Alfvénic Mach number $\mathrm{M_A} = 6.9$ as in Run 1, the quasi-perpendicular portion of the bow shock lies roughly at the same distance from Earth both in the $x-y$ and the $x-z$ planes, while its quasi-parallel sector is found closer to Earth, according 135 to MHD simulations (Chapman et al., 2004). Therefore, if the IMF lies in the $x-z$ plane, the position and shape of the bow shock in this plane are essentially the same as those observed in the equatorial plane for an IMF vector in the $x-y$ plane. Since the main parameter controlling magnetosheath asymmetries is the bow shock configuration (Dimmock et al., 2017), the IMF configuration in Run 1 is roughly equivalent to a Parker spiral IMF orientation in terms of bow shock and outer magnetosheath properties (i.e. away from the cusps and the reconnecting magnetopause). We will therefore use this run as a reference for the 140 most typical IMF orientation at Earth. The other set of two runs, Runs 2A and 2B, are equatorial runs, with a $30°$ cone angle IMF in the $x-y$ plane. In Run 2A, the IMF strength is set to 5 nT, as in Run 1, while in Run 2B, its value is set to 10 nT. As a result, the Alfvén Mach number $\mathrm{M_A}$ is reduced to 3.5 in this run, half of its value in Runs 1 and 2A where $\mathrm{M_A} = 6.9$. To avoid confusion in the case where the simulation plane is not the equatorial plane, we will refer to the polarity of the magnetosheath asymmetries as $\mathrm{Q}_\perp$-favoured or $\mathrm{Q}_\parallel$-favoured, instead of the dawn-dusk terminology generally used in observational studies.

145 In each run, we divide the dayside magnetosheath into sectors within which we calculate the average magnetosheath properties, as illustrated by the black curves in Figure 1a. In a global simulation, the magnetopause position can be obtained from the deflection of the magnetosheath flow pattern around the magnetosphere (see, for example, Palmroth et al., 2018). This method

is however impractical to analyse a large number of simulation time steps as is done here, and our analysis does not require the exact magnetopause position. Therefore, we use for simplicity the same shape as that of the Shue et al. (1997) magnetopause

150 model (of the form $r = r_0(2/(1 + \cos\theta))^\alpha$), where r_0 is the stand-off distance, θ the angle from the Sun-Earth line and α the flaring parameter, to delineate the boundaries of the bins in the radial direction. This shape approximates relatively well the bow shock and magnetopause shape in our simulations when different flaring parameters are used.

For each run, the values for $r_0 = r_{\min}$ (inner boundary), $r_0 = r_{\max}$ (outer boundary) and α are selected by visual inspection so as to maximise the coverage of the magnetosheath while remaining sufficiently far from the bow shock and the magne-

155 topause to avoid including data from other regions. The two intermediate radial boundaries are placed at one third and two thirds of the magnetosheath thickness $r_{\max} - r_{\min}$. We denote the relative position between the magnetosheath boundaries as $F_{\text{Msheath}} = (r - r_{\min})/(r_{\max} - r_{\min})$. In the azimuthal direction, the magnetosheath is divided into 18 10°-wide angular bins. In our analysis, we will only focus on the central and outer sets of radial bins, to ensure that the cusps are excluded and that magnetopause processes do not affect our results in Run 1.

160 Inside each of these bins, we calculate the average values of various magnetosheath parameters, namely the ion density, the plasma bulk velocity and the magnetic field strength. In addition to spatial averages within each bin, we also perform temporal averages in order to minimise the effects of transient features originating from the foreshock or arising inside the magnetosheath. Here we use 150 s temporal averages to calculate the magnetosheath parameters, which was found as a good trade-off to remove the effect of transients with only limited changes in the position of the magnetosheath boundaries. This is

165 comparable with the 180 s window used by Dimmock et al. (2017) for spacecraft measurements. We note here that because of the 2D set-up of our simulations, field lines tend to pile-up at the magnetopause, as they cannot slip along the magnetosphere flanks. As a result, the bow shock moves slowly outwards. To ensure that the comparison of the different runs is meaningful, we select time intervals in Run 1 and Run 2A when the bow shock shape was comparable, as it should not be strongly affected by the different IMF cone angles. In Run 1, we calculate the average magnetosheath parameters between $t = 700$ and $t = 850$ s,

170 when the simulation has properly initialised and before the onset of intense dayside reconnection, which could cause changes in the flow pattern near the magnetopause, and to limit the effects of reconnection-driven magnetic islands in the magnetosheath (Pfau-Kempf et al., 2016). In Runs 2A and 2B, we use the interval from $t = 350$ to $t = 500$ s. The initialisation phase of these runs is shorter than in Run 1 because of their smaller simulation domain.

Following Dimmock et al. (2017), we define the asymmetry of the magnetosheath parameters as:

175 $$A = 100 \times \left(\frac{Q_\perp - Q_\parallel}{Q_\perp + Q_\parallel} \right) \qquad (1)$$

where $Q_\perp$ is the average value of a magnetosheath parameter (here magnetic field strength, plasma velocity or ion density) in a given azimuthal and radial bin in the quasi-perpendicular magnetosheath, and $Q_\parallel$ its average value in the corresponding opposite bin, i.e., symmetric with respect to the Sun-Earth line, in the quasi-parallel magnetosheath. Note that we use the same arrangement of quasi-perpendicular and quasi-parallel bins in the analysis of Runs 2A and 2B, even though the reduced cone

180 angle in these runs shifts the transition between the two shock regimes away from the bow shock nose. This facilitates the

comparison with observational studies, which do not account for the IMF cone angle in their mapping of the magnetosheath parameters (e.g. Dimmock et al., 2017).

3 Results

3.1 Magnetic field strength

185   Colour-coded in the top panels of Figure 1 is the magnetic field strength in the dayside magnetosheath and the neighbouring regions, normalised to the IMF strength, in each of the three runs. As indicated by the magnetic field lines (light grey curves), the quasi-parallel sector of the bow shock and its associated foreshock extend in the lower part of each plot, upstream of the southern ($z < 0$, in Run 1) or dawnside ($y < 0$, in Runs 2A and 2B) magnetosheath. The colour scheme is chosen to highlight the areas of the magnetosheath where the normalised magnetic field strength is above or below 4, which is the upper limit for the

190   magnetic field compression at the bow shock crossing according to the Rankine-Hugoniot jump conditions (Treumann, 2009). In Run 2B, the normalised magnetic field strength is below 4 in most of the magnetosheath, due to the weaker compression at the bow shock when the Alfvén Mach number is low. In Runs 1 and 2A, it remains below 4 in the first few Earth radii ($R_E = 6371$ km) downstream of the subsolar bow shock, and in a much broader area in the flank magnetosheath. In regions closer to the magnetopause, its values increase well above 4 due to the field lines piling up in front of the magnetosphere.

195   In the subsolar region, the effects of pile-up are visible even in the outermost magnetosheath bins used in our study (black curves), while they are limited to the central and inner magnetosheath bins further on the flanks. They also extend further out in the quasi-perpendicular magnetosheath than downstream of the quasi-parallel shock, due to the IMF orientation. Similar features due to pile-up are also observed in the statistical maps compiled by Dimmock et al. (2017) (see the top panels of their Figure 5.1). The only significant difference between our simulation results and Dimmock et al. (2017)'s maps is the large

200   magnetic field strength along the northern magnetopause close to the terminator in Run 1, which is likely due to the 2D set-up of our simulation, resulting in enhanced field line pile-up. In the following, we will exclude from our analysis the innermost magnetosheath bins and concentrate on the central and outer magnetosheath properties.

    The bottom panels of Figure 1 show the asymmetry (see Eq. 1) of the magnetic field strength in the central ($1/3 < F_{\mathrm{Msheath}} < 2/3$) and outer ($2/3 < F_{\mathrm{Msheath}} < 1$) magnetosheath as a function of the angle from the Sun-Earth line. The asymmetry level is

205   obtained from both a spatial average of this parameter inside each azimuthal bin and a temporal average over 150 s of the simulation, in order to minimise the effects of transient structures in the magnetosheath. Figures 1d and e reveal a definite $Q_\perp$-favoured asymmetry (positive values of the asymmetry) in all three runs. In Run 1, which corresponds to a typical Parker-spiral IMF orientation at Earth, we find an average asymmetry of 9%. The asymmetry is also significantly weaker in the central magnetosheath than just downstream of the shock, suggesting that the field line draping and pile-up in front of the magnetosphere

210   tend to smooth out the effects of the bow shock. Our results are in good agreement with the 5% $Q_\perp$-favoured asymmetry obtained by Dimmock et al. (2017) based on statistics of spacecraft data. This $Q_\perp$-favoured asymmetry is due to the stronger compression of the magnetic field at the quasi-perpendicular bow shock, because only the tangential magnetic field compo-
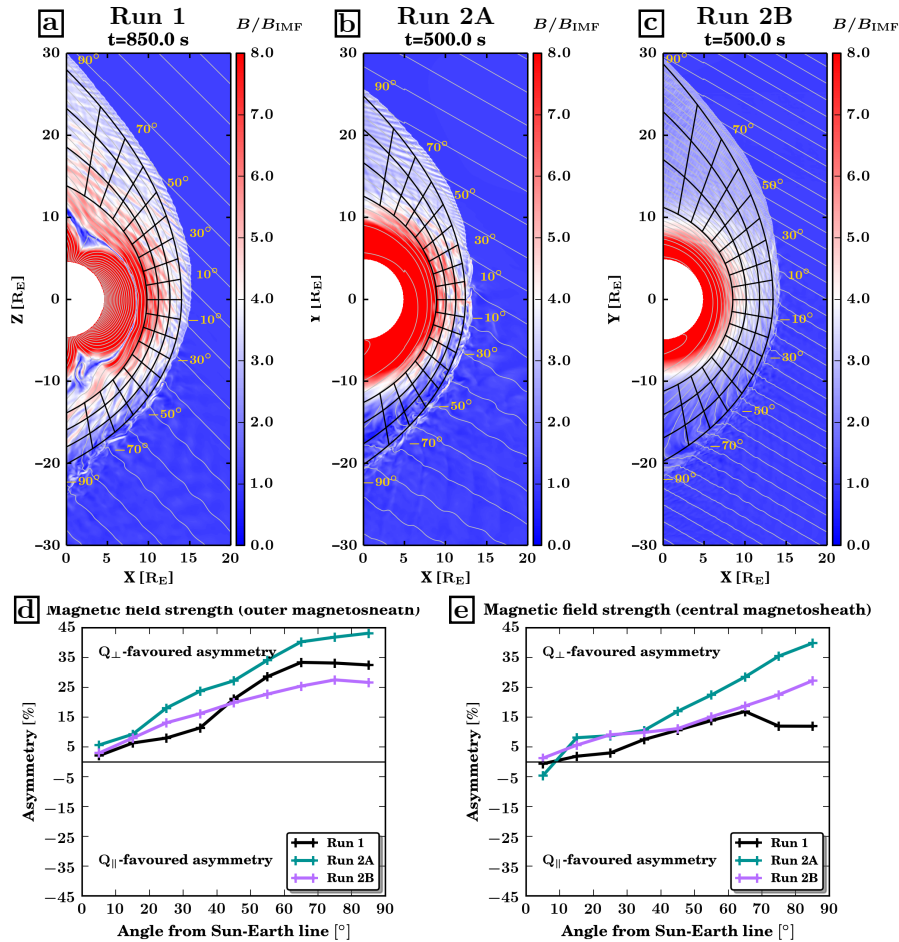
Figure 1. Top panels: magnetic field strength in the simulation plane, normalised with the IMF strength, in Run 1 at time $t = 850$ s (a), in Run 2A (b) and 2B (c) at time $t = 500$ s. The light grey lines show magnetic field lines. The spatial bins used to calculate the average magnetosheath parameters are shown in black. Bottom panels: magnetic field strength asymmetry in the central (d) and outer (e) magnetosheath.

nents are enhanced at the bow shock crossing, while the normal component remains unchanged (Treumann, 2009; Hoilijoki et al., 2019).

215   When the cone angle is reduced from $45°$ to $30°$ in Runs 2A and 2B, the asymmetry becomes stronger in the central magnetosheath, exceeding 40% on the flanks in Run 2A. This is most likely due to the quasi-parallel sector of the shock being shifted closer to the subsolar point, and thus affecting a larger fraction of the dayside magnetosheath. As a result, the regions of very low magnetic field strength (in dark blue in the bottom parts of panels a-c), due to the weak magnetic field compression at the quasi-parallel shock crossing, extend over most of the dawn side magnetosheath, forming a starker contrast with the dusk

220   sector. We also note that they penetrate deeper in the magnetosheath, resulting in similar levels of magnetic field asymmetry in
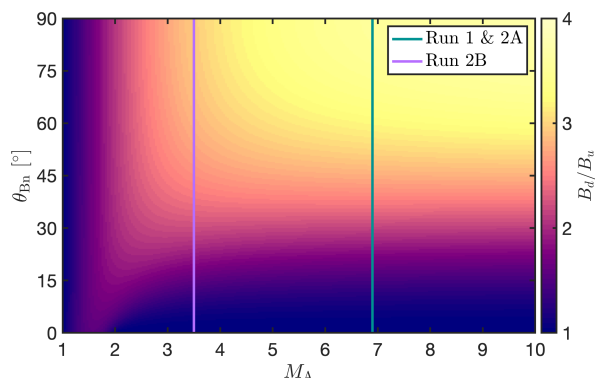
Figure 2. Downstream to upstream ratio of the magnetic field strength as a function of M_A and θ_{Bn}, calculated based on the Rankine-Hugoniot relations.

the outer and the central magnetosheath in Runs 2A and 2B. This contrast between Run 1 and Runs 2A and 2B may be related to the different draping pattern of the field lines at lower cone angle.

The magnetic field asymmetry is significantly weaker in Run 2B than in Run 2A. This lower asymmetry level at lower M_A is most likely due to the reduced magnetic field compression affecting more strongly the magnetic field strength downstream

225 of the quasi-perpendicular bow shock. To confirm this, we calculate the magnetic field strength just downstream of the bow shock based on the Rankine-Hugoniot jump conditions and assuming magnetic coplanarity is satisfied. We use the solar wind parameters of the Vlasiator runs as upstream conditions. The downstream to upstream ratio of the magnetic field magnitude is displayed in Figure 2 as a function of θ_{Bn} and M_A. This clearly shows that the magnetic field compression at the quasi-parallel bow shock does not vary with M_A for the considered M_A range, while higher values are reached on the quasi-perpendicular

230 side as M_A increases. These different behaviours on the quasi-parallel and the quasi-perpendicular sectors as a function of M_A result in a less pronounced asymmetry at lower M_A.

Finally, we observe a gradual increase in the asymmetry from the subsolar region towards the flanks. This is likely due to the variation of the θ_{Bn} angle along the bow shock surface. In Run 1, θ_{Bn} increases from the bow shock nose to the terminator on the quasi-perpendicular side, while it decreases at a similar rate on the quasi-parallel side, reaching its extrema ($0°$ and $90°$) on

235 both flanks in the last azimuthal bin near the terminator. In Runs 2A and 2B, θ_{Bn} also increases with the azimuthal angle on the quasi-perpendicular side, but on the quasi-parallel sector, it first decreases until reaching 0 at around $45°$ from the Sun-Earth line, and then starts increasing again. The magnetic field asymmetry keeps increasing beyond this point probably because the asymmetry level is computed in a broad area and not just in the close vicinity of the bow shock, and other effects than shock compression come into play in the magnetosheath, for example field line pile-up and draping around the magnetosphere.
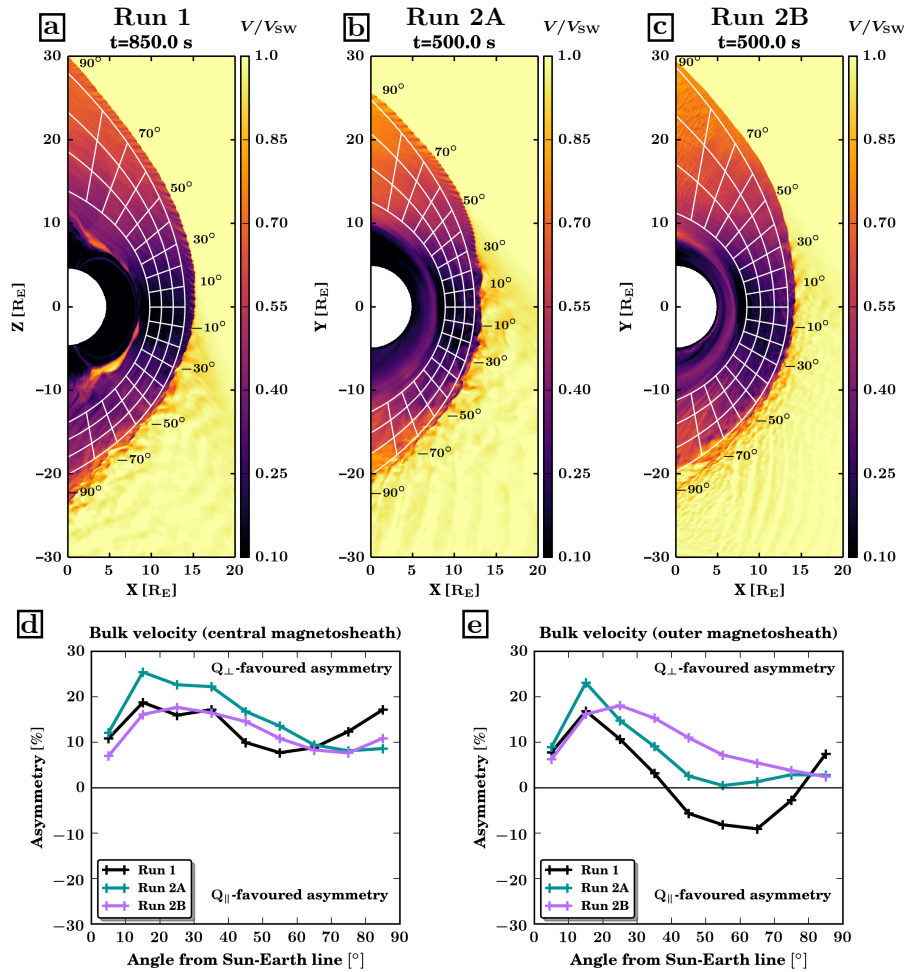
Figure 3. Top panels: ion bulk velocity in the simulation plane, normalised with the solar wind speed, in Run 1 at time $t = 850\,\mathrm{s}$ (a), in Run 2A (b) and 2B (c) at time $t = 500$ s. The spatial bins used to calculate the average magnetosheath parameters are shown in black. Bottom panels: magnetic field strength asymmetry in the central (d) and outer (e) magnetosheath.

3.2 Ion bulk velocity

Figure 3 displays the plasma bulk velocity normalised to the solar wind speed in the three runs, and its associated asymmetry in the central and outer magnetosheath, in the same format as Figure 1. Again, the asymmetry is calculated based on a 150 s average of the bulk velocity inside each of the magnetosheath bins. As expected, the plasma velocity is very low in the subsolar magnetosheath, while the flow is faster on the flanks, because the tangential velocity is mostly preserved at the shock while its normal component is reduced, according to Rankine-Hugoniot relations.

Figure 3d shows a pronounced $Q_\perp$-favoured asymmetry in the central magnetosheath, with velocities 13% higher on average in the quasi-perpendicular flank in Run 1 and in Run 2B. In Run 2A, very high values, over 25%, are reached in some azimuthal

bins close to the subsolar region. However, the average level of the asymmetry is 15% in the central magnetosheath, only marginally higher than in the other runs. Dimmock and Nykyri (2013) and Dimmock et al. (2017) evidenced a $Q_\perp$-favoured

250 asymmetry in their statistical data set, albeit with values somewhat below those found in our simulations, between 5 and 10%. Walsh et al. (2012) also reported a velocity asymmetry with the same polarity in spacecraft measurements and in MHD simulations.

In the outer magnetosheath, the level of the asymmetry tends to decrease when moving away from the subsolar region. As illustrated in Fig. 4, which shows the average velocity in the outer magnetosheath as a function of the angle from the Sun-Earth

255 line, the flow speed increases more rapidly on the quasi-parallel flank than on the quasi-perpendicular flank. This progressively smoothes out the difference between both sectors. Also, the fact that the velocity is larger further down on the flanks tends to reduce the asymmetry level, as the same absolute difference in velocity between the quasi-parallel and quasi-perpendicular sectors results in a smaller value of the asymmetry, which is calculated as the relative difference (see Eq. 1).

In Run 1, the reduction in the asymmetry level causes a reversal of the asymmetry polarity from $Q_\perp$- to $Q_\parallel$-favoured

260 beyond $40°$ from the Sun-Earth line, while the asymmetry is close to 0 in Run 2A. Only in Run 2B does the asymmetry remain persistently $Q_\perp$-favoured across the entire dayside magnetosheath. These different asymmetry polarities in the outer magnetosheath in the azimuthal bins beyond $40°$ from the Sun-Earth line reflect a much steeper increase in the flow speeds on the quasi-parallel flank in Run 1 than in Runs 2A and 2B. This likely stems from the irregular shape of the bow shock in Run 1, which bulges outward beyond $-70°$ from the Sun-Earth line due to a large and persistent foreshock transient. On the

265 other hand, the more pronounced asymmetry in Run 2B than in Run 2A is caused by the dependence of the shock compression ratio on the Alfvén Mach number and the θ_{Bn} angle. Figure 5 displays the shock compression ratio as a function of θ_{Bn} for the two different M_A values in Runs 2A and 2B. As illustrated in Fig. 5, the shock compression ratio is roughly constant over the whole θ_{Bn} range for the M_A of Run 2A (in green), while it is considerable lower on the quasi-perpendicular side than on the quasi-parallel side at the lower M_A of Run 2B (in purple). This explains the reduced asymmetry level in Run 2A compared to

270 Run 2B.

Our simulations also show that the flow stagnation region is slightly shifted from the subsolar point towards the quasi-parallel magnetosheath (see Fig. 4). In Run 1, the velocity minimises at about $10°$ from the Sun-Earth line on the quasi-parallel side. This is probably due to the velocity deflection at the bow shock which depends on θ_{Bn}, as predicted by the Rankine-Hugoniot jump conditions to preserve the continuity of the tangential electric field (e.g., Treumann, 2009). As a result, asymmetric flow

275 speeds are observed when comparing the quasi-perpendicular and quasi-parallel magnetosheath. Field line draping around the magnetosphere may also play a role in reducing the velocity in the quasi-parallel magnetosheath. The shift of the stagnation region towards the quasi-parallel flank is slightly greater for a $30°$ cone angle (Runs 2A and 2B), consistent with the θ_{Bn} dependence of the velocity deviation at the bow shock.

3.3 Ion density

280 Plotted in Fig. 6 is the ion density and its associated asymmetry in the central and outer magnetosheath, in the same format as Figures 1 and 3. The upper panels show that the ion density in the magnetosheath is essentially up to four times its upstream
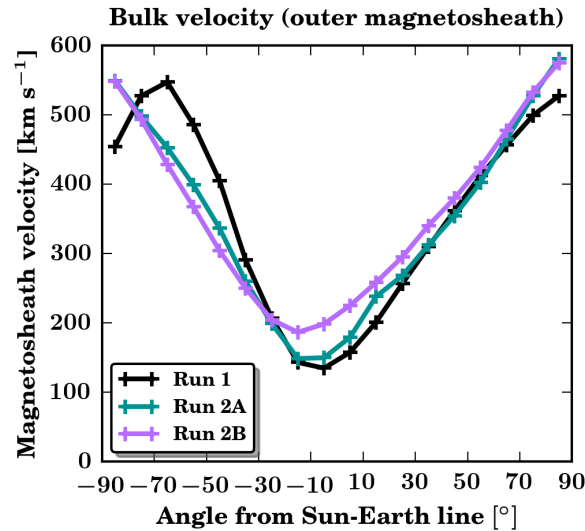
Figure 4. Bulk velocity in the outer magnetosheath as a function of the angle from the Sun-Earth line in all three runs.
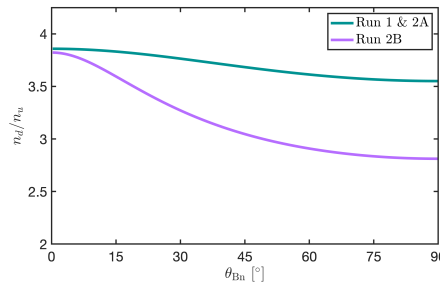
Figure 5. Density compression ratio as a function of θ_{Bn} for two different M_A values, corresponding to those in the simulation runs.

value, consistent with previous works and with the theoretical plasma compression ratio at the bow shock (Formisano et al., 1973). A few regions of larger density enhancements (in yellow) are observed downstream of the quasi-parallel shock, probably due to dynamical processes associated with the foreshock or the quasi-parallel shock. Similar transient density enhancements
285 are seen throughout the 150 s of simulated time which are used to calculate the magnetosheath asymmetry.

Figures 6d and 6e evidence a mostly $Q_\parallel$-favoured asymmetry of the ion density in the magnetosheath. Multiple azimuthal bins display however an opposite polarity of the asymmetry. Moreover, we note that the values of the density asymmetry are much more sensitive to the time interval over which the data are averaged than for the other parameters under study. This is probably due to the variability of the plasma density just downstream of the quasi-parallel shock. The patches of high density
290 alternate with depleted regions, which result in $Q_\perp$-favoured asymmetries in some azimuthal bins, even when performing long temporal averages. This demonstrates the high variability of the magnetosheath density, even under completely steady solar wind conditions. For example, in Run 2A, we note that patches of high density just downstream of the bow shock are
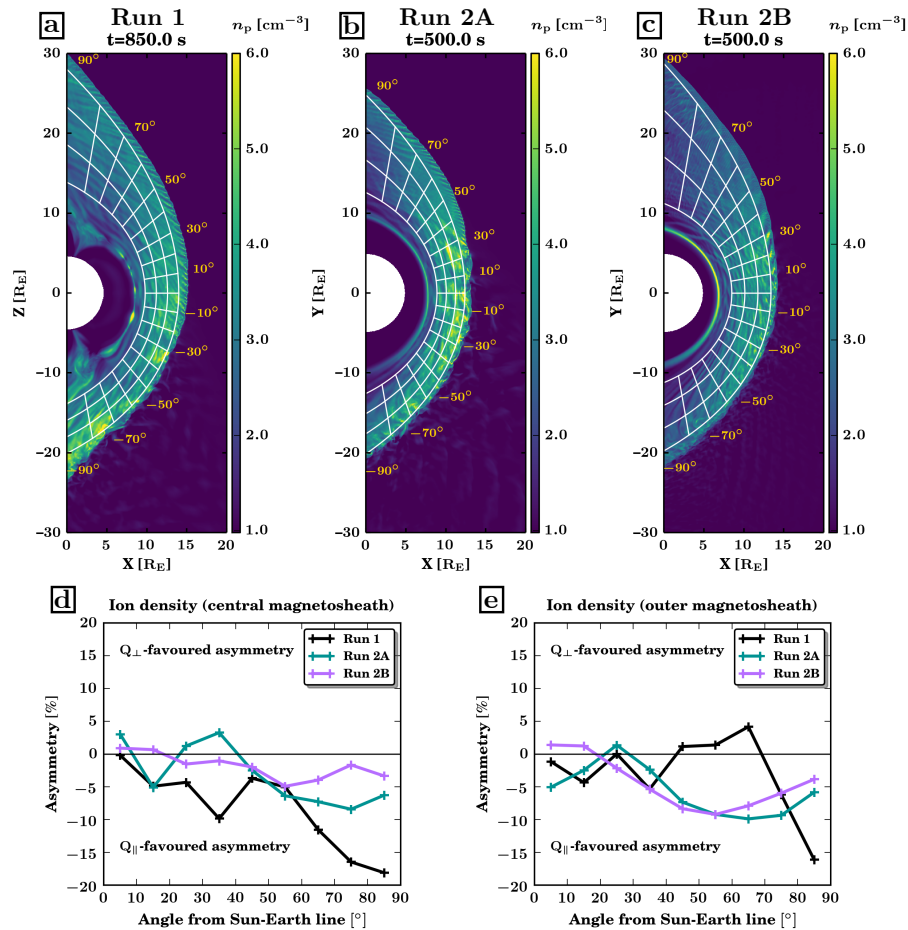
Figure 6. Same format as in Figure 3 but for the ion density.

concentrated in the subsolar magnetosheath and are distributed on either sides of the Sun-Earth line, as evidenced in Figure 6b. This could explain the reversed polarity of the asymmetry in some azimuthal bins near the subsolar point.

295   Comparing the asymmetry levels in the different runs, we find that the median value in the central magnetosheath is -5% both in Run 1 and Run 2A, and reduces (in absolute value) to -2% in Run 2B. As mentioned in Section 3.2, the shock compression ratio shows little dependence on θ_{Bn} in the range of M_A associated with Runs 1 and 2A, while it is significantly lower on the quasi-perpendicular flank than on the quasi-parallel flank in the low M_A range, such as in Run 2B. Therefore, according to the MHD theory, the density asymmetry should be stronger at lower M_A, which contradicts our numerical results.

300   The different behaviour in our simulation hints at kinetic effects playing a dominant role.

     Finally, we note that the variability of the density in the outer magnetosheath is much lower at reduced M_A, which results in a smoother distribution of the asymmetry, leading to a steadily $Q_{\parallel}$-favoured asymmetry for all azimuthal bins beyond $20°$ from

the Sun-Earth line in Run 2B. This could be related to foreshock disturbances being weaker at lower M_A, since the density of suprathermal ions is reduced (Turc et al., 2015, 2018).

305 3.4 Comparison with spacecraft observations

We now compare our numerical results with the asymmetries obtained from a statistical data set of magnetosheath observations from the Time History of Events and Macroscale Interactions during Substorms (THEMIS) spacecraft (Angelopoulos, 2008; Dimmock and Nykyri, 2013; Dimmock et al., 2017). The data were collected between January 2008 and December 2017 and are binned according to the spacecraft coordinates in the Magnetosheath InterPlanetary Medium (MIPM) reference frame

310 (Bieber and Stone, 1979; Dimmock et al., 2017). In this coordinate system, the $x-$axis points opposite to the solar wind flow, while the $y-$axis is defined such that the quasi-perpendicular sector of the bow shock lies in the $+y$ direction and its quasi-parallel sector at negative y. This ensures that all data associated with a given shock regime are grouped together on one side of the magnetosheath. The $z-$axis completes the orthogonal set. Then the radial coordinate of each measurement point is calculated as the fractional distance between a model bow shock and magnetopause, which removes the effects of the motion of

315 these boundaries due to changing upstream conditions. The data points are thus organised with their fractional distance inside a normalised magnetosheath and with their azimuthal angle from the Sun-Earth line. Each measurement point is associated with a set of upstream conditions, based on the OMNI data (King and Papitashvili, 2005) at the time of the THEMIS observations. More details on the data processing can be found in Dimmock and Nykyri (2013); Dimmock et al. (2017) and the references therein.

320 As in previous studies using this statistical data set (e.g. Dimmock et al., 2015a; Dimmock et al., 2017), we concentrate only on measurements in the central magnetosheath, that is, where $1/3 < F_{\mathrm{Msheath}} < 2/3$, to avoid including data from other regions in case of inaccuracies in the determination of the boundary position. The average parameters in the central magnetosheath are computed inside $15°$-wide angular bins, with a 50% overlap between two consecutive bins. The asymmetry is then calculated using Eq. 1. Furthermore, we divide the statistical data set into two ranges of cone angles, depending on the IMF orientation

325 associated with each of the magnetosheath measurements. The magnetosheath asymmetries associated with a cone angle close to that of the Parker spiral orientation ($40° < \theta_{\mathrm{Bx}} < 50°$) are shown in black in Figure 7 and those associated with a lower cone angle value ($20° < \theta_{\mathrm{Bx}} < 35°$) are plotted in blue. We note here that the data set contained too few data points at $M_A < 5$ for us to investigate the change in the asymmetries at low Alfvén Mach number.

Firstly, we find an excellent agreement between simulations and observations regarding the polarity of the asymmetry for the

330 three parameters considered here, as noted already in the previous sections. The levels of asymmetry tend however to be lower in the observational data compared to the simulations. This could be due to the processing method of the statistical data set, which calculates averages over very diverse upstream conditions, and thus results in a conservative estimate of the asymmetry.

As concerns the influence of the cone angle, the statistical data do not show evidence of a significant increase of the magnetic field strength asymmetry when the cone angle is reduced, contrary to our numerical simulations. The median value of the

335 asymmetry marginally decreases, from 2.6% to 2.2%, when restricting the data set to cone angles between 20 and $35°$. On

the other hand, the bulk velocity asymmetry becomes slightly more pronounced at lower cone angles, with a median value increasing from 4.7 to 5.1%, consistent with the small increase found in Run 2A.

The density asymmetry displays much more spatial variability at low cone angle, with about half of the azimuthal bins having a $Q_\perp$-favoured asymmetry, while most of them showed a clear $Q_\parallel$-favoured asymmetry for a Parker spiral IMF orientation. This
340 agrees well with the numerical results presented above, and is likely due to foreshock processes causing enhanced variability of the magnetosheah density at lower cone angles. Because of this reversed polarity in many azimuthal bins, the median value of the asymmetry is close to 0 for low cone angle values, instead of about -3% for $40-50°$ cone angles.

4 Discussion

We have quantified the asymmetry of the magnetic field magnitude, ion density and bulk flow velocity inside the dayside mag-
345 netosheath in three Vlasiator global runs with different IMF conditions. We note that the use of global numerical simulations presents two main advantages.

First, the global coverage of the magnetosheath for a given set of solar wind conditions provided by the simulations allows us to investigate the asymmmetries both in the central and the outer magnetosheath. In contrast, observational studies are often restricted to the central magnetosheath to make sure that the data set does not include magnetosphere or solar wind
350 measurements (e.g. Dimmock et al., 2015a; Dimmock et al., 2017), or to locations just outside the magnetopause to avoid relying on boundary models to estimate the position inside the magnetosheath (Walsh et al., 2012). The comparison of the asymmetry levels in the central and outer magnetosheath provides us with new information regarding the influence of the bow shock and foreshock on the magnetosheath parameters, and in particular shows the importance of transient foreshock processes.

Second, the simulations enable us to investigate the asymmetry levels at low Alfvén Mach number ($M_A \sim 3.5$, Run 2B),
355 while the statistical data set compiled from THEMIS measurements does not contain enough data points at such low M_A to derive the asymmetry of the magnetosheath parameters. This is why we did not compare our numerical results concerning M_A with observations in Section 3.4. Low Alfvén Mach numbers are encountered only occasionally at Earth, but they are of great importance for solar wind-magnetosphere coupling because they are associated with extreme solar wind disturbances such as magnetic clouds (Turc et al., 2016) and they result in atypical conditions in the magnetosheath (Lavraud et al., 2013). Other
360 studies have suggested that the Alfvén Mach number plays a role in the asymmetry (Walsh et al., 2012; Dimmock et al., 2017) but it is difficult to make a direct and meaningful comparison between all of these studies since there are extensive differences across methodologies, models, and datasets. However, there are clearly unanswered questions which deserve further study and may be addressed with future missions and/or model runs.

The main limitation of our numerical simulations is the 2D set-up, which results in particular in enhanced field line pile-
365 up in front of the magnetopause, and thus causes an outward motion of the bow shock. We verified that this does not affect significantly the asymmetry levels, and found that the variability of the asymmetries in the simulation was caused by transient processes rather than by the shock progressive expansion. The 2D set-up may also influence the field line draping pattern in the magnetosheath, which could strengthen the magnetic field decrease in the central magnetosheath on the quasi-parallel

flank. Future 3D simulations could allow to evaluate if the asymmetry is less pronounced in this region than in the outer

370 magnetosheath when field lines can flow around the magnetosphere.

We note that the levels of asymmetry obtained from the numerical simulations are larger than those from the observational data set, for all parameters considered in this study. This is probably due to the fundamentally different methods through which the magnetosheath parameters were obtained. In the simulations, the asymmetry is calculated based on spatial averages of the magnetosheath parameters for a single set of steady upstream conditions, while observational results are a compilation of

375 localised measurements taken during a variety of upstream conditions. Specifically, the IMF can assume any orientation in the observational data set, including in particular an out-of-plane component while the THEMIS spacecraft orbit near the Earth's equatorial plane. Even though the MIPM reference frame arranges the measurements corresponding to the quasi-parallel/quasi-perpendicular sectors on the negative/positive $y-$hemispheres, it does not account for the different cone angles nor for the out-of-plane IMF component. As a result, data points associated with widely different θ_{Bn} values can be grouped together. Also,

380 some data points may be misidentified as quasi-parallel or quasi-perpendicular because the upstream conditions are determined from the OMNI propagated data set which may not reflect exactly the actual conditions at Earth's bow shock. These two effects would tend to smooth out the asymmetries in the statistical data set. The numerical simulations, on the other hand, do not suffer from these limitations, resulting in more pronounced asymmetries. The apparent discrepancy between observations and simulations is only a natural consequence of the different methods used for obtaining the average magnetosheath parameters.

385 The magnetic field asymmetry also behaves differently in the observations and the simulations when changing the cone angle. In Vlasiator, we find a significant increase of the asymmetry at low cone angle, whereas it marginally decreases in the statistical THEMIS data set. It should be noted that the spacecraft observations are not associated with a single value of the IMF cone angle, but are a compilation of measurements taken for a range of cone angles, between 20 and $35°$. As the IMF becomes more radial, the quasi-parallel sector of the bow shock and its associated foreshock move closer to the subsolar point.

390 For a purely radial IMF, the magnetosheath asymmetries due to the bow shock configuration should completely disappear, as the θ_{Bn} values are then distributed symmetrically about the Sun-Earth line (see e.g. Turc et al., 2016). Therefore, there should be a value of the cone angle at which the magnetosheath asymmetries maximise, before decreasing when further reducing the cone angle to finally reach the symmetrical configuration for a purely radial IMF. The range of cone angles used in collating the statistical data might therefore contain significant variation in asymmetry levels. This in turn could explain why on average

395 the asymmetry level for $20 - 35°$ cone angles remains the same as for $40 - 50°$ cone angles in the observations.

Using a semi-empirical model of the magnetosheath magnetic field (Turc et al., 2014), we calculate the asymmetry level of the magnetic field strength associated with the same upstream parameters as in Run 1 and Run 2A. The model predicts a higher asymmetry level at $30°$ than at $45°$ cone angle (not shown), in agreement with our numerical simulations. This lends further support to the hypothesis that the different behaviour in spacecraft measurements could be due to the array of solar wind

400 conditions and IMF orientations included in the statistical data set. Also, the data could be affected by processes at snaller spatial scales than those resolved in our simulations, though it is unlikely that this will play a significant role here, since the data are averaged over several minutes.

The ion density asymmetry was essentially $Q_\parallel$-favoured in all our runs, consistent with previous observational and numerical works (Paularena et al., 2001; Longmore et al., 2005; Walsh et al., 2012; Dimmock et al., 2016b) and MHD theory (Walters, 1964). It should be noted however that the most recent studies by Dimmock et al. (2016b) and Dimmock et al. (2017) only found a clear $Q_\parallel$-favoured asymmetry near the magnetopause, while no clear polarity was observed in the central magnetosheath. In our simulations, we found in many instances that the asymmetry in some of the azimuthal bins displayed an opposite polarity. We also observed a large temporal variability of both its level and its polarity in our simulations, despite the completely steady upstream conditions. This suggests that the magnetosheath density is extremely sensitive to transient processes, originating for example in the foreshock. The fluctuations that are typically present in the solar wind parameters would be conducive to even more variability of the magnetosheath density. The inconclusive results regarding the polarity of this asymmetry in the central magnetosheath (Dimmock et al., 2016b; Dimmock et al., 2017) and the large discrepancies in the asymmetry levels quantified in various studies (see the summary table in Walsh et al., 2014) likely stem from this high variability.

5 Conclusions

In this work, we studied the asymmetry between the quasi-parallel and the quasi-perpendicular sectors of the Earth's magnetosheath using global hybrid-Vlasov simulations. We quantified the level of asymmetry in the central and outer magnetosheath for the magnetic field strength, ion density and bulk velocity and investigated its variation when reducing the cone angle and the M_A. For all parameters, we find a polarity of the asymmetry ($Q_\perp$-favoured or $Q_\parallel$-favoured) that is consistent with earlier works (see Dimmock et al., 2017, for a recent review). The asymmetry levels tend to be higher in the numerical simulations, due to the fact that the magnetosheath parameters are obtained for a given set of fixed upstream conditions in the model, instead of a compilation of normalised localised measurements.

For a $30°$ cone angle, we found similar levels of asymmetry in the outer and central magnetosheath, while they differed significantly at a larger cone angle. We also noted that there was more variability of the density asymmetry in the central magnetosheath. This suggests that transient foreshock processes have an effect deeper in the magnetosheath when the foreshock is located closer to the subsolar point. The magnetic field strength asymmetry increased significantly at $30°$ cone angle, possibly due to the low θ_{Bn} near the bow shock nose resulting in a reduced magnetic field compression across most of the quasi-parallel flank of the magnetosheath. This effect was however not observed in the statistical data sets.

Reducing the M_A results in a less pronounced magnetic field asymmetry because of the weaker compression of the magnetic field at the quasi-perpendicular bow shock, while that at the quasi-parallel shock remains roughly unchanged. We also noted that the velocity and density asymmetries display less variability, probably due to weaker foreshock disturbances at lower M_A. This change is particularly visible here because of the low cone angle, but may be less discernable for less radial IMF orientations, as the foreshock will retreat towards the flank. Future simulation runs with a low M_A and a larger cone angle could allow to test this.

It is worth noting that even for completely steady upstream conditions, the magnetosheath density shows significant temporal variations, in particular downstream of the quasi-parallel shock. These variations are likely caused by foreshock transient

processes. They can influence noticeably the level of asymmetry in some parts of the magnetosheath, and even cause reversals of its polarity in some azimuthal sectors. Our results show that density asymmetry variations in the magnetosheath are an inherent effect of the bow shock and foreshock, instead of a statistical artefact. This is most likely one of the sources for the wide variety of levels of density asymmetry quantified in previous observational studies.

440   This work shows that global kinetic simulations provide a reliable tool to study magnetosheath asymmetries. The global coverage of the magnetosheath obtained in each run allows for a precise quantification of the asymmetry levels for a given set of solar wind conditions, in contrast with spacecraft statistical data sets which quantify the average value of the asymmetries across a wide range of upstream conditions. Moreover, the inclusion of ion kinetic physics is necessary to properly describe foreshock processes which affect strongly the variability of the magnetosheath density. Numerical simulations also enable us

445   to perform parametric studies, thus allowing us to study the influence of specific upstream parameters. Here we limited our analysis to three runs because of the large computational cost of Vlasiator simulations, but future studies could make use of larger sets of runs, with more varied upstream conditions, once they become available.

Code availability.   Vlasiator (http://www.helsinki.fi/en/researchgroups/vlasiator/, Palmroth, 2020) is distributed under the GPL-2 open source license at http://github.com/fmihpc/vlasiator/ (Palmroth and the Vlasiator team, 2020). Vlasiator uses a data structure developed in-house

450   (https://github.com/fmihpc/vlsv/, Sandroos, 2019), which is compatible with the VisIt visualization software (Childs et al., 2012) using a plugin available at the VLSV repository. The Analysator software (https://github.com/fmihpc/analysator/, Hannuksela and the Vlasiator team, 2020) was used to produce the presented figures. The runs described here take several terabytes of disk space and are kept in storage maintained within the CSC – IT Center for Science. Data presented in this paper can be accessed by following the data policy on the Vlasiator web site.

455   *Author contributions.*   L.T. initiated and coordinated the study, performed part of the data analysis and wrote the first draft of the manuscript. V.T. developed the methodology and performed the initial data analysis. A.D. provided the THEMIS statistical data set and helped in the interpretation of the results. A.J. provided Figures 2 and 5, and contributed to the comparison with the Rankine-Hugoniot jump conditions. M.P. is the PI of the Vlasiator model and gave inputs to the interpretation of the simulation results. M.B., U.G. and Y.P.-K. ran the Vlasiator runs used in this study. Together with A.J., M.G. and M.D., they contributed to the analysis of the Vlasiator outputs. All co-authors

460   participated in the discussion of the results and contributed to improving the manuscript.

Competing interests.   The authors declare that they have no conflict of interest.

Acknowledgements.   This project has received funding from the European Union's Horizon 2020 research and innovation programme under the Marie Sklodowska-Curie grant agreement No 704681. The work of L.T. is supported by the Academy of Finland (grant number

322544). We acknowledge the European Research Council for Starting grant 200141-QuESpace, with which Vlasiator was developed, and

465 Consolidator grant 682068-PRESTISSIMO awarded to further develop Vlasiator and use it for scientific investigations. The work leading to

these results has been carried out in the Finnish Centre of Excellence in Research of Sustainable Space (Academy of Finland grant numbers

312351 and 312390). We acknowledge PRACE Tier-0 grant number 2016153521 with which Run 1 was carried out in CINECA, Italy. The

CSC - IT Center for Science in Finland is acknowledged for the Grand Challenge awards leading to the results shown here for Runs 2A and

2B.

470 **References**

Angelopoulos, V.: The THEMIS Mission, Space Sci. Rev., 141, 5–34, https://doi.org/10.1007/s11214-008-9336-1, 2008.

Bieber, J. W. and Stone, S. C.: Energetic electron bursts in the magnetopause electron layer and in interplanetary space., in: Magnetospheric Boundary Layers, edited by Battrick, B., Mort, J., Haerendel, G., and Ortner, J., vol. 148 of *ESA Special Publication*, pp. 131–135, 1979.

Chapman, J. F., Cairns, I. H., Lyon, J. G., and Boshuizen, C. R.: MHD simulations of Earth's bow shock: Interplanetary magnetic field orienta-
475 tion effects on shape and position, Journal of Geophysical Research (Space Physics), 109, A04215, https://doi.org/10.1029/2003JA010235, 2004.

Childs, H., Brugger, E., Whitlock, B., Meredith, J., Ahern, S., Pugmire, D., Biagas, K., Miller, M., Harrison, C., Weber, G. H., Krishnan, H., Fogal, T., Sanderson, A., Garth, C., Bethel, E. W., Camp, D., Rübel, O., Durant, M., Favre, J. M., and Navrátil, P.: VisIt: An End-User Tool For Visualizing and Analyzing Very Large Data, in: High Performance Visualization–Enabling Extreme-Scale Scientific Insight, pp.
480 357–372, Chapman & Hall / CRC, 2012.

Daldorff, L. K. S., Tóth, G., Gombosi, T. I., Lapenta, G., Amaya, J., Markidis, S., and Brackbill, J. U.: Two-way coupling of a global Hall magnetohydrodynamics model with a local implicit particle-in-cell model, Journal of Computational Physics, 268, 236–254, https://doi.org/10.1016/j.jcp.2014.03.009, 2014.

Dimmock, A. P. and Nykyri, K.: The statistical mapping of magnetosheath plasma properties based on THEMIS measurements in
485 the magnetosheath interplanetary medium reference frame, Journal of Geophysical Research (Space Physics), 118, 4963–4976, https://doi.org/10.1002/jgra.50465, 2013.

Dimmock, A. P., Nykyri, K., and Pulkkinen, T. I.: A statistical study of magnetic field fluctuations in the dayside magnetosheath and their dependence on upstream solar wind conditions, Journal of Geophysical Research (Space Physics), 119, 6231–6248, https://doi.org/10.1002/2014JA020009, 2014.

490 Dimmock, A. P., Nykyri, K., Karimabadi, H., Osmane, A., and Pulkkinen, T. I.: A statistical study into the spatial distribution and dawn-dusk asymmetry of dayside magnetosheath ion temperatures as a function of upstream solar wind conditions, Journal of Geophysical Research (Space Physics), 120, 2767–2782, https://doi.org/10.1002/2014JA020734, 2015a.

Dimmock, A. P., Osmane, A., Pulkkinen, T. I., and Nykyri, K.: A statistical study of the dawn-dusk asymmetry of ion temperature anisotropy and mirror mode occurrence in the terrestrial dayside magnetosheath using THEMIS data, Journal of Geophysical Research (Space
495 Physics), 120, 5489–5503, https://doi.org/10.1002/2015JA021192, 2015b.

Dimmock, A. P., Nykyri, K., Osmane, A., and Pulkkinen, T. I.: Statistical mapping of ULF Pc3 velocity fluctuations in the Earth's dayside magnetosheath as a function of solar wind conditions, Advances in Space Research, 58, 196–207, https://doi.org/10.1016/j.asr.2015.09.039, 2016a.

Dimmock, A. P., Pulkkinen, T. I., Osmane, A., and Nykyri, K.: The dawn-dusk asymmetry of ion density in the dayside magnetosheath and
500 its annual variability measured by THEMIS, Annales Geophysicae, 34, 511–528, https://doi.org/10.5194/angeo-34-511-2016, 2016b.

Dimmock, A. P., Nykyri, K., Osmane, A., Karimabadi, H., and Pulkkinen, T. I.: Dawn-Dusk Asymmetries of the Earth's Dayside Mag-netosheath in the Magnetosheath Interplanetary Medium Reference Frame, chap. 5, pp. 49–72, American Geophysical Union (AGU), https://doi.org/10.1002/9781119216346.ch5, https://agupubs.onlinelibrary.wiley.com/doi/abs/10.1002/9781119216346.ch5, 2017.

Eastwood, J. P., Nakamura, R., Turc, L., Mejnertsen, L., and Hesse, M.: The Scientific Foundations of Forecasting Magnetospheric Space
505 Weather, Space Science Reviews, 212, 1221–1252, https://doi.org/10.1007/s11214-017-0399-8, 2017.

Formisano, V., Hedgecock, P. C., Moreno, G., Palmiotto, F., and Chao, J. K.: Solar wind interaction with the Earth's magnetic field: 2. Magnetohydrodynamic bow shock, Journal of Geophysical Research, 78, 3731, https://doi.org/10.1029/JA078i019p03731, 1973.

Hannuksela, O. and the Vlasiator team: Analysator: python analysis toolkit, Github repository, https://github.com/fmihpc/analysator/, last access: 09.03.2020, 2020.

510 Hoilijoki, S., Ganse, U., Sibeck, D. G., Cassak, P. A., Turc, L., Battarbee, M., Fear, R. C., Blanco-Cano, X., Dimmock, A. P., Kilpua, E. K. J., Jarvinen, R., Juusola, L., Pfau-Kempf, Y., and Palmroth, M.: Properties of Magnetic Reconnection and FTEs on the Dayside Magnetopause With and Without Positive IMF B_x Component During Southward IMF, Journal of Geophysical Research (Space Physics), 124, 4037–4048, https://doi.org/10.1029/2019JA026821, 2019.

King, J. H. and Papitashvili, N. E.: Solar wind spatial scales in and comparisons of hourly Wind and ACE plasma and magnetic field data,
515 Journal of Geophysical Research (Space Physics), 110, A02104, https://doi.org/10.1029/2004JA010649, 2005.

Lavraud, B., Larroque, E., Budnik, E., Génot, V., Borovsky, J. E., Dunlop, M. W., Foullon, C., Hasegawa, H., Jacquey, C., Nykyri, K., Ruffenach, A., Taylor, M. G. G. T., Dandouras, I., and Rème, H.: Asymmetry of magnetosheath flows and magnetopause shape during low Alfvén Mach number solar wind, Journal of Geophysical Research (Space Physics), 118, 1089–1100, https://doi.org/10.1002/jgra.50145, 2013.

520 Longmore, M., Schwartz, S. J., Geach, J., Cooling, B. M. A., Dandouras, I., Lucek, E. A., and Fazakerley, A. N.: Dawn-dusk asymmetries and sub-Alfvénic flow in the high and low latitude magnetosheath, Annales Geophysicae, 23, 3351–3364, https://doi.org/10.5194/angeo-23-3351-2005, 2005.

Lucek, E. A., Constantinescu, D., Goldstein, M. L., Pickett, J., Pinçon, J. L., Sahraoui, F., Treumann, R. A., and Walker, S. N.: The Magnetosheath, Space Science Reviews, 118, 95–152, https://doi.org/10.1007/s11214-005-3825-2, 2005.

525 Němeček, Z., Šafránková, J., Zastenker, G. N., Pišoft, P., and Paularena, K. I.: Spatial distribution of the magnetosheath ion flux, Advances in Space Research, 30, 2751–2756, https://doi.org/10.1016/S0273-1177(02)80402-1, 2002.

Němeček, Z., M., H., Šafránková, J., Zastenker, G. N., and Richardson, J. D.: The dawn-dusk asymmetry of the magnetosheath: INTERBALL-1 observations, Advances in Space Research, 31, 1333 – 1340, https://doi.org/https://doi.org/10.1016/S0273-1177(03)00007-3, 2003.

530 Nykyri, K., Ma, X., Dimmock, A., Foullon, C., Otto, A., and Osmane, A.: Influence of velocity fluctuations on the Kelvin-Helmholtz instability and its associated mass transport, Journal of Geophysical Research (Space Physics), 122, 9489–9512, https://doi.org/10.1002/2017JA024374, 2017.

Palmroth, M.: Vlasiator, Web site, https://www.helsinki.fi/en/researchgroups/vlasiator/, last access: 09.03.2020, 2020.

Palmroth, M. and the Vlasiator team: Vlasiator: hybrid-Vlasov simulation code, Github repository, https://github.com/fmihpc/vlasiator/,
535 version 5.0, last access: 09.03.2020, 2020.

Palmroth, M., Ganse, U., Pfau-Kempf, Y., Battarbee, M., Turc, L., Brito, T., Grandin, M., Hoilijoki, S., Sandroos, A., and von Alfthan, S.: Vlasov methods in space physics and astrophysics, Living Reviews in Computational Astrophysics, 4, 1, https://doi.org/10.1007/s41115-018-0003-2, 2018.

Paularena, K. I., Richardson, J. D., Kolpak, M. A., Jackson, C. R., and Siscoe, G. L.: A dawn-dusk density asymmetry in Earth's magneto-
540 sheath, Journal of Geophysical Research, 106, 25 377–25 394, https://doi.org/10.1029/2000JA000177, 2001.

Petrinec, S. M., Mukai, T., Nishida, A., Yamamoto, T., Nakamura, T. K., and Kokubun, S.: Geotail observations of magnetosheath flow near the magnetopause, using Wind as a solar wind monitor, Journal of Geophysical Research, 102, 26 943–26 960, https://doi.org/10.1029/97JA01637, 1997.

Pfau-Kempf, Y., Hietala, H., Milan, S. E., Juusola, L., Hoilijoki, S., Ganse, U., von Alfthan, S., and Palmroth, M.: Evidence for transient, local ion foreshocks caused by dayside magnetopause reconnection, Annales Geophysicae, 34, 943–959, https://doi.org/10.5194/angeo-34-943-2016, 2016.

Pulkkinen, T. I., Dimmock, A. P., Lakka, A., Osmane, A., Kilpua, E., Myllys, M., Tanskanen, E. I., and Viljanen, A.: Magnetosheath control of solar wind-magnetosphere coupling efficiency, Journal of Geophysical Research (Space Physics), 121, 8728–8739, https://doi.org/10.1002/2016JA023011, 2016.

Sandroos, A.: VLSV: file format and tools, Github repository, https://github.com/fmihpc/vlsv/, last access: 09.03.2020, 2019.

Shue, J. H., Chao, J. K., Fu, H. C., Russell, C. T., Song, P., Khurana, K. K., and Singer, H. J.: A new functional form to study the solar wind control of the magnetopause size and shape, Journal of Geophysical Research (Space Physics), 102, 9497–9512, https://doi.org/10.1029/97JA00196, 1997.

Soucek, J., Escoubet, C. P., and Grison, B.: Magnetosheath plasma stability and ULF wave occurrence as a function of location in the magnetosheath and upstream bow shock parameters, Journal of Geophysical Research (Space Physics), 120, 2838–2850, https://doi.org/10.1002/2015JA021087, 2015.

Spreiter, J. R., Summers, A. L., and Alksne, A. Y.: Hydromagnetic flow around the magnetosphere, Planetary and Space Science, 14, https://doi.org/10.1016/0032-0633(66)90124-3, 1966.

Treumann, R. A.: Fundamentals of collisionless shocks for astrophysical application, 1. Non-relativistic shocks, Astronomy and Astrophysics Review, 17, 409–535, https://doi.org/10.1007/s00159-009-0024-2, 2009.

Turc, L., Fontaine, D., Savoini, P., and Kilpua, E. K. J.: A model of the magnetosheath magnetic field during magnetic clouds, Ann. Geophys., 32, 157–173, https://doi.org/10.5194/angeo-32-157-2014, 2014.

Turc, L., Fontaine, D., Savoini, P., and Modolo, R.: 3D hybrid simulations of the interaction of a magnetic cloud with a bow shock, Journal of Geophysical Research (Space Physics), 120, 6133–6151, https://doi.org/10.1002/2015JA021318, 2015.

Turc, L., Escoubet, C. P., Fontaine, D., Kilpua, E. K. J., and Enestam, S.: Cone angle control of the interaction of magnetic clouds with the Earth's bow shock, Geophysical Research Letters, 43, 4781–4789, https://doi.org/10.1002/2016GL068818, 2016.

Turc, L., Ganse, U., Pfau-Kempf, Y., Hoilijoki, S., Battarbee, M., Juusola, L., Jarvinen, R., Brito, T., Grandin, M., and Palmroth, M.: Foreshock Properties at Typical and Enhanced Interplanetary Magnetic Field Strengths: Results From Hybrid-Vlasov Simulations, Journal of Geophysical Research (Space Physics), 123, 5476–5493, https://doi.org/10.1029/2018JA025466, 2018.

von Alfthan, S., Pokhotelov, D., Kempf, Y., Hoilijoki, S., Honkonen, I., Sandroos, A., and Palmroth, M.: Vlasiator: First global hybrid-Vlasov simulations of Earth's foreshock and magnetosheath, Journal of Atmospheric and Solar-Terrestrial Physics, 120, 24–35, https://doi.org/10.1016/j.jastp.2014.08.012, 2014.

Walsh, A. P., Haaland, S., Forsyth, C., Keesee, A. M., Kissinger, J., Li, K., Runov, A., Soucek, J., Walsh, B. M., Wing, S., and Taylor, M. G. G. T.: Dawn-dusk asymmetries in the coupled solar wind-magnetosphere-ionosphere system: a review, Annales Geophysicae, 32, 705–737, https://doi.org/10.5194/angeo-32-705-2014, 2014.

Walsh, B. M., Sibeck, D. G., Wang, Y., and Fairfield, D. H.: Dawn-dusk asymmetries in the Earth's magnetosheath, Journal of Geophysical Research (Space Physics), 117, A12211, https://doi.org/10.1029/2012JA018240, 2012.

Walters, G. K.: Effect of Oblique Interplanetary Magnetic Field on Shape and Behavior of the Magnetosphere, Journal of Geophysical Research, 69, 1769–1783, https://doi.org/10.1029/JZ069i009p01769, 1964.

Wang, Y., Raeder, J., and Russell, C.: Plasma depletion layer: Magnetosheath flow structure and forces, Annales Geophysicae, 22, 1001–1017, https://doi.org/10.5194/angeo-22-1001-2004, 2004.

Wing, S., Johnson, J. R., Newell, P. T., and Meng, C. I.: Dawn-dusk asymmetries, ion spectra, and sources in the northward interplanetary magnetic field plasma sheet, Journal of Geophysical Research (Space Physics), 110, A08205, https://doi.org/10.1029/2005JA011086, 2005.
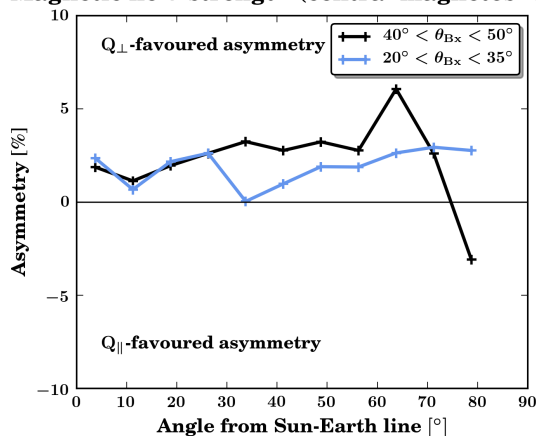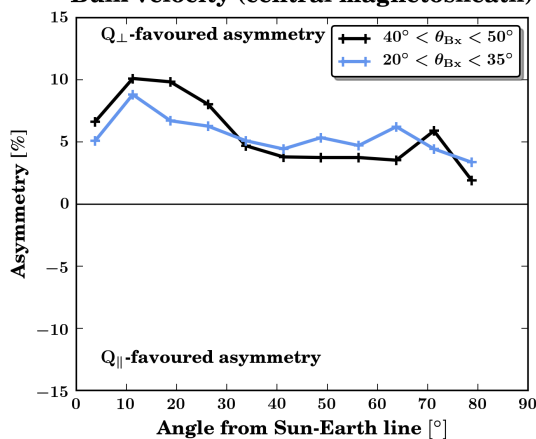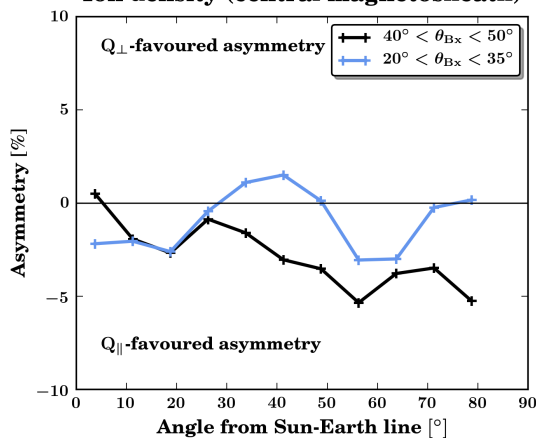
Figure 7. Asymmetries in the central magnetosheath as obtained from statistics of THEMIS spacecraft observations. From top to bottom: magnetic field strength, bulk velocity and ion density. The black curves correspond to data with a cone angle near the Parker spiral orientation ($40° < \theta_{\mathrm{Bx}} < 50°$) and the blue curves to data with a low cone angle values ($20° < \theta_{\mathrm{Bx}} < 35°$).